International Conference on Space Optics—ICSO 2000
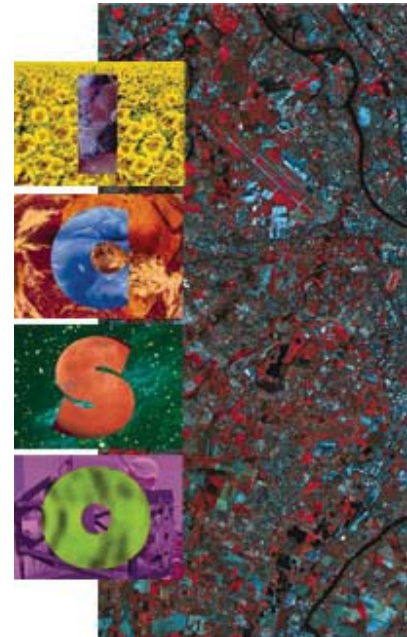
Toulouse Labège, France

5–7 December 2000

Effect of telescope antenna diagram on the data acquisition in a stellar interferometer

Emmanuel Longueteau, Laurent Delage, François Reynaud

EFFECT OF TELESCOPE ANTENNA DIAGRAM ON THE DATA ACQUISITION IN A STELLAR INTERFEROMETER

Emmanuel LONGUETEAU, Laurent DELAGE, François REYNAUD
Equipe optique, IRCOM(UMR 6615),123, avenue A.Thomas, 87060 LIMOGES cedex-FRANCE-

Résumé: Cet article présente l'étude de l'influence du diamètre des télescopes sur la qualité des données collectées par un interféromètre stellaire à fibre otique. A cette occasion nous utilisons la notion de diagramme d'antenne fréquemment utilisée en micro-ondes. Ce concept est fondamental pour expliquer les dégradations induites sur les mesures de clôtures de phase et de contrastes effectuées par un interféromètre stellaire. Le défaut de pointage des télescopes vient s'ajouter au problème de champ et peut devenir critique

Abstract: This paper deals with the effect of the telescope size on accuracy of the data acquisition in a optical fibre linked stellar interferometer. In this context we introduce the concept of antenna diagram commonly used for micro-waves antennae. This concept is essential to explain the contrasts and the phase-closure acquisitions corruption in a stellar interferometer. The telescope pointing errors induces additional effects that are superimposed with the field limitation and could become critical.

1-INTRODUCTION

In the frame of an ESA contract (OAST2) on high resolution imaging, IRCOM institute manufactured a scale model telescope array in order to test an end to end demonstrator of image acquisition by means of a fibre linked synthesised aperture. The emerging data consist of three contrasts and one phase-closure measurements relative to the telescopes triplets involved in each elementary array. These contrasts and phase-closure are samples of object spectrum at the spatial frequencies defined by the telescopes bases. From these partial information on the object spectrum the image reconstruction can be achieved using self-calibrated Wipe or Maximum entropy algorithms. [Dela 00]

The experimentation of this scale model points out a problem caused by the telescope size. When large telescope input pupils are used, the complex visibility measurements are corrupted and very sensitive to pointing errors. In order to reduce this defect we have inserted masks in front of each telescope to reduce the clear aperture and make the measurement more reliable. In one hand this technique allows us to collect uncorrupted data but in the other hand the light flux collected by the telescopes becomes very low. This trade-off brings us to study the telescope size effect on the phase-closure measurement and visibility function acquisition and their correlative effects on the image reconstruction.

2-OVERVIEW OF THE HIGH RESOLUTION IMAGING TEST BENCH.

2.1-Description of the test bench:

The scale model of stellar interferometer developed at IRCOM (fig1) consists of three subassemblies [Dela 00]:

-     The stellar object simulator:
This object consists of 24 optical fibres glued side by side. They are located in the focus plane of the collimator and fed by independent laser diodes. In such way, the object is spatially incoherent and its intensity can be easily managed.
-     The object monitoring:
The object is directly imaged by a CCD-camera held in the telescope focus. It allows us to obtain a reference image of the observed object.
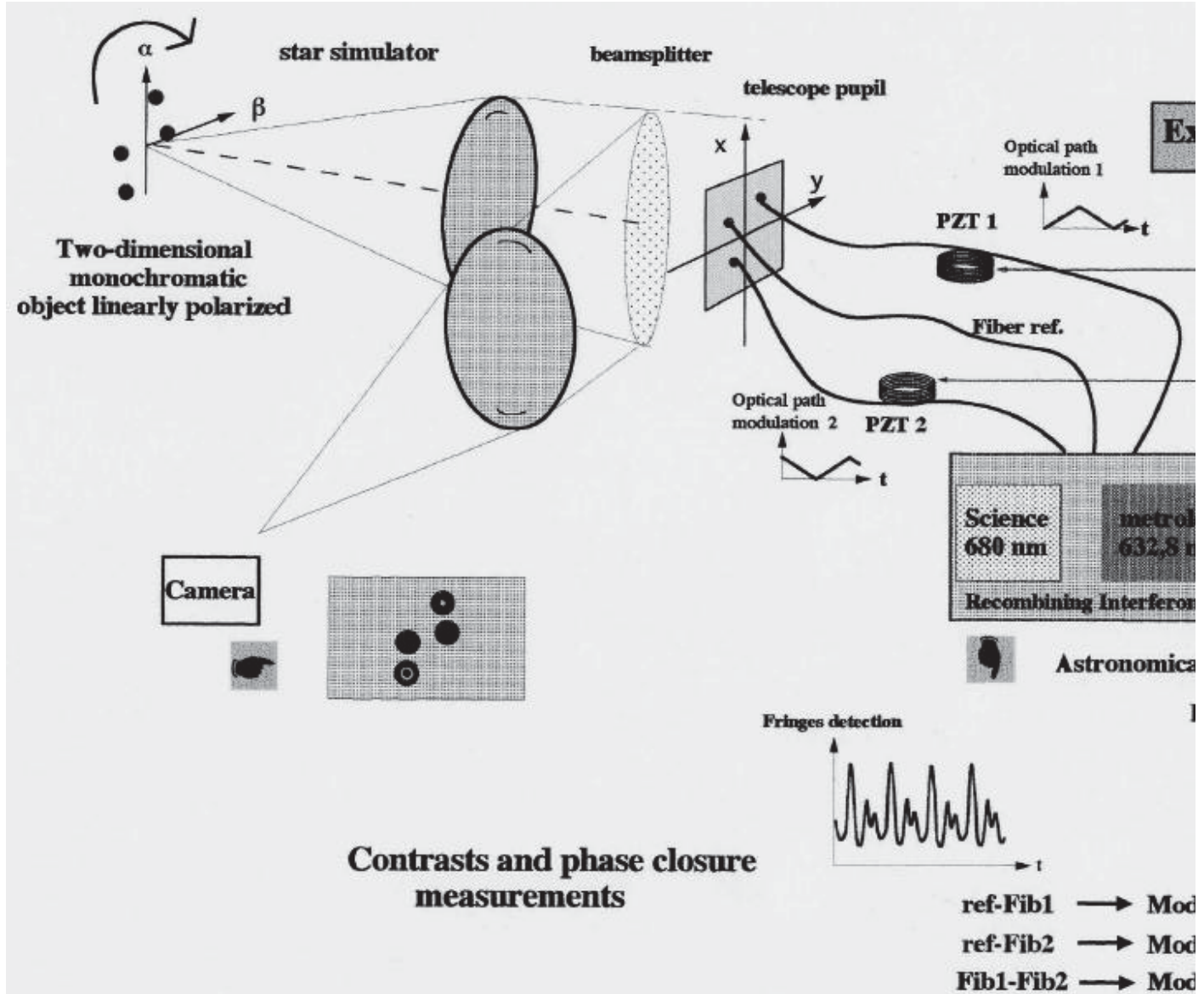-   The stellar interferometer:
The optical field coming from the star simulator is launched into three polarisation maintaining fibres by means of three lens acting as telescopes. Two optical fibres are linearly stretched by piezo-electric modulator in order to generate three various optical path between the three fibre arms. After recombination, we observe three interference fringe patterns allowing to measure the complex visibility. By reconfiguring the three apertures, it is possible to sample the spatial frequency plane in order to collect the required data for the image reconstruction.

2.2-Typical experimental results and relevant problems:

This scale model has been experimented by Laurent Delage and François Reynaud from IRCOM institute. The optical path in the interferometer is controlled with a 5nm accuracy. For each array configuration the emerging data results from an averaging over 30 snap shot measurements. The RMS fluctuation of the phase closure is typically 10^{-2} rad. However, with 5 mm diameter lens, the telescope pointing defaults (less 20 arc second) induce larger phase closure variations. This behaviour results from the angular resolution of each telescope leading to a spatial selection on the object. In order to decrease these fluctuations, we have to insert masks in front of lenses to deteriorate the spatial resolution of each telescopes. With 1,5 mm clear aperture the data became reliable and the image reconstruction have been achieved successfully. Of course the reduction of telescope clear aperture leads to a collected flux decrease.

In the next paragraph we investigate this behaviour by using the concept of telescope antenna diagram.

Fig 1

3-TELESCOPE ANTENNA DIAGRAM

3.1-Definition of the antenna diagram:

The concept of antenna diagram must be introduced to explain the data corruption in the frame of stellar interferometry. The antenna diagram is defined as the normalised electromagnetism power emitted or received in a given direction. When operating for emission or reception, the antenna diagram does not change for a given antenna.

With optical beams, the intensity antenna diagram can be defined as the normalised photometric intensity distribution emitted or received by an antenna in a given direction [Kudi 97]. We can also define the field antenna diagram as the square root of the antenna diagram i.e. the normalised distribution of the electric field modulus. In the following we will study the association of a telescope and a monomode optical fibre. The input of the wave-guide is located in the focal plane of the light collector. This assembly will be characterised by its intensity or field antenna diagram.

The telescope intensity antenna diagram $R(\theta,\varphi)$ can be written:

$$R(\theta,\varphi) = \frac{I(\theta,\phi)}{I_{max}}$$

Where θ and φ define the observed direction.

$I(\theta,\varphi)$ (Watt/steradian) the photometric intensity emerging in (θ, φ) direction,

and I_{max} be the maximum emission intensity

3.2-Experimental measurement of an aperture antenna diagram:

The following part describes the experimental test bench used for antenna diagram measurement and the corresponding results.

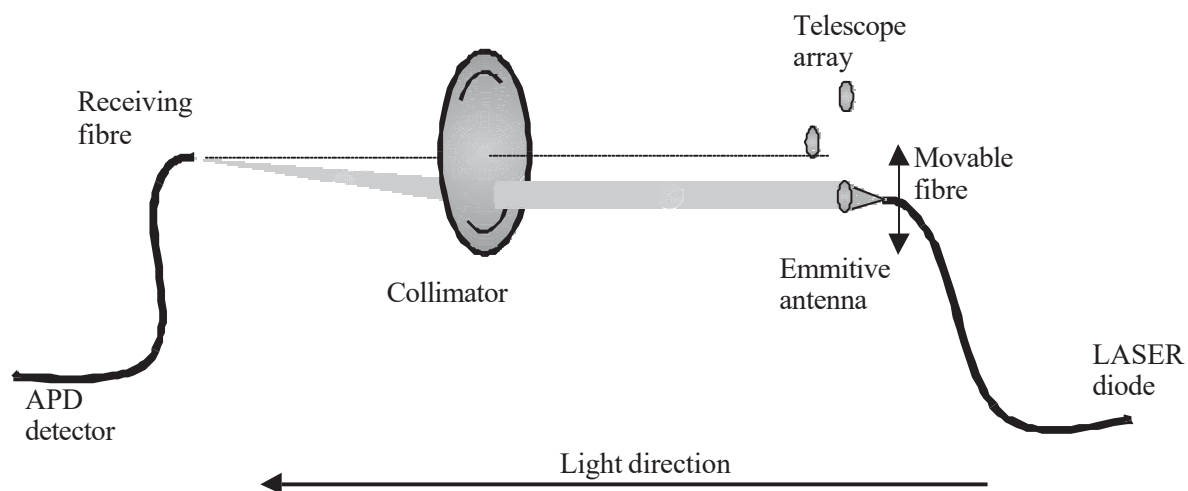#### 3.2.1-Experimental configuration:

fig2 : experimental characterisation of the antenna diagram .

The experimental acquisition of the intensity antenna diagram use a backward propagation of the light emitted by a laser diode and launched in the fibre at the interferometric mixing output. The emitting fibre is translated in the telescope focal plane in order to scan all emission directions.

The far field of this antenna is observed in the focal plane of a collimator. An optical fibre connected to an avalanche photodiode, is placed at the focus of the collimator and allows to measure photometric intensity versus direction.

3.2.2-Experimental results:

The experimental results and simulations are shown in figure 3. This 1D-antenna diagram curves are recorded or computed for 1,5 and 5 mm aperture diameters.
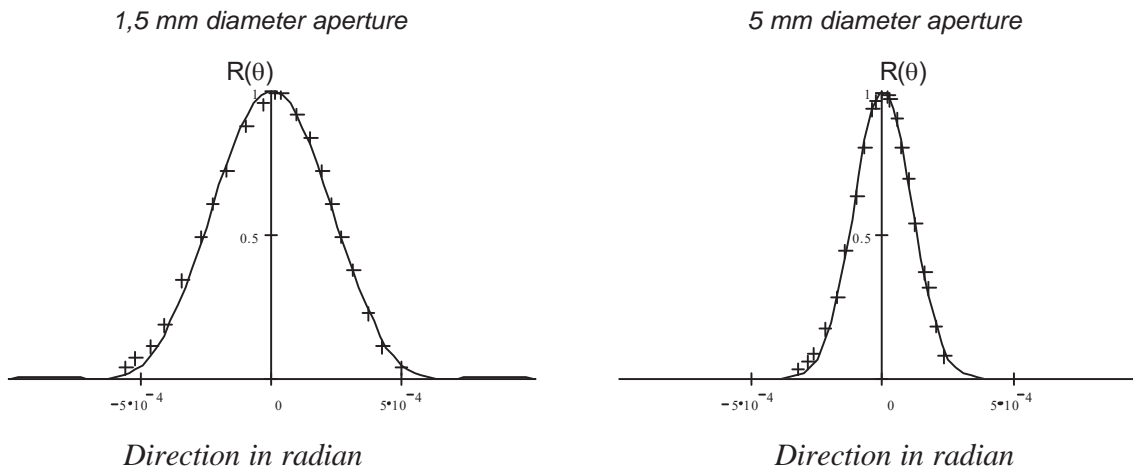

fig 3 :1D-antenna diagram measurements with emissive antenna R(θ)
+ experimental measurement
——simulation curves

Numerical simulation fit accurately the experimental results for the 1,5 and 5 mm diameter assuming a beam with a gaussian shape. The experimental widths of the antenna diagram are in the range of 10^{-4} rad in our laboratory prototype with a 10 mm focal lens.

4-PROBLEM: CORRUPTION OF THE COMPLEX VISIBILITY FUNCTION

4.1-Theoretical study:

4.1.1-Biased Zernike and Van Cittert theorem:

In order to explain data corruption, the problem will be simplified by considering a two telescope interferometer and a one-dimensional object.

Interference function for a monochromatic point-like source dI and for two apertures:
Let b be the distance between the two apertures
The fringe pattern can be expressed by the following relation:

$$\text{dmeasure} = d\theta.I(\theta)\ (1 + k.a1.a2.\cos(\omega t + \frac{2\pi\theta b}{\lambda}))$$

Where K is the instrumental visibility factor , ω the temporal frequencies (pulsation) of fringes, λ the wavelength of the source and θ is the direction of the source element.

The a1 and a2 factors are the photometric coefficient of each arm of the interferometer depending on the light to fibre coupling i.e. the antenna diagram. a1 and a2 are θ dependant and include the pointing errors.

After integration over all the source the interference function becomes:

$$measure = I_0 + Re(\int k.I(\theta).a1(\theta).a2(\theta).e^{2\pi j\frac{\theta b}{\lambda}} d\theta)\cos(\omega t)$$

In the case of a1 and a2 are equal to 1, we found the Zernike and Van Cittert theorem [Born 80]. The influence of the a1(θ) and a2(θ) coefficient on the image to be carefully investigated. The following paragraphs demonstrate the data corruption as function of the telescope fields and pointing errors.

4.1.2-Corruption induced by the antenna diagram width:

For an ideal acquisition device a1 and a2 are constant so that the measure only give information on object spectrum. The following graph (fig 6) show an object to be provided by our test bench. This curve displays the angular intensity distribution I(θ) of the triplet object. It will be used for all the numerical simulations.
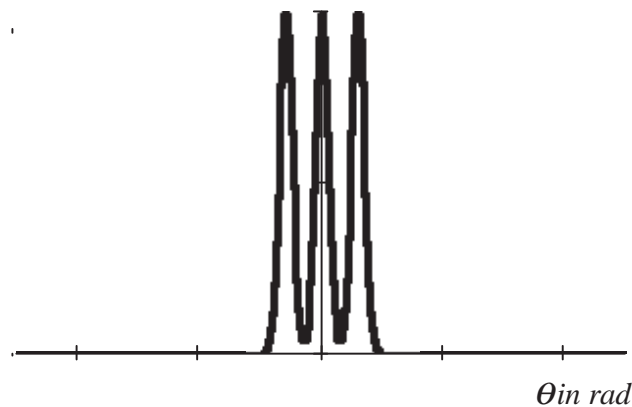

θ in rad

fig 6: angular object intensity distribution I(θ) versus θ

Taking the effect of the antenna diagram into account, the information collected correspond to the a1(θ).a2(θ).I(θ) product. Assuming no telescope pointing defaults, the product is represented on the figure 7 is the observable object. Computations have been achieved using the 1,5 and 5 mm antenna diagrams and the experimental framework of our test bench.

1,5 mm diameter aperture

5 mm diameter aperture
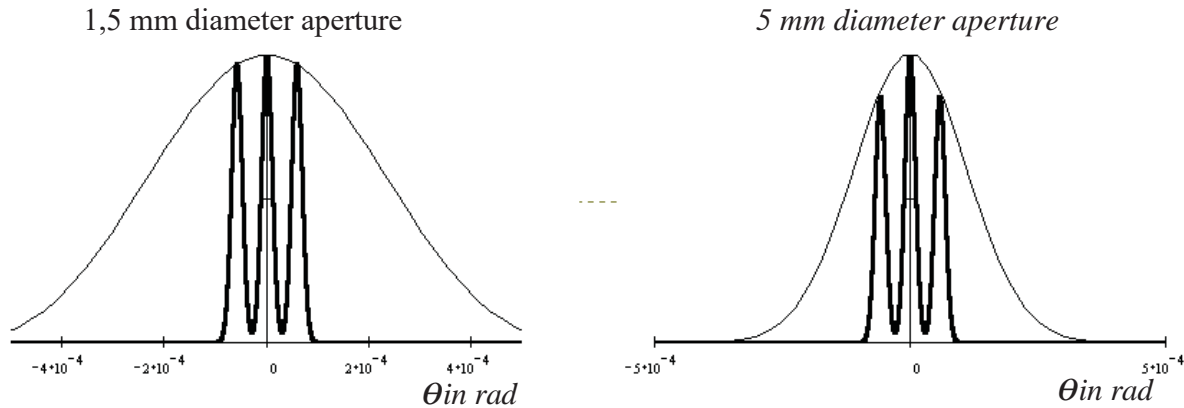
fig 7:effect of antenna diagram on the observable object (product a1(θ).a2(θ).I(θ))
sharp curves: field antenna diagram a1(θ) = a2(θ)
bold curves: a1(θ).a2(θ).I(θ) product

With a 1,5 mm diameter the relative error between the two maximum is 4% conversely to the 5 mm diameter aperture that give an 15 %relative error.

Figure 7 demonstrates that with large telescopes the object measurements are biased because each aperture is beginning to resolve the object. The larger the telescope diameter the stronger this effect.

Note that the knowledge of the a1(θ) and a2(θ).antenna diagram coefficients allows to unbias the data as long as these coefficient do not reach too small values.

4.1.3-Corruption induced by a telescope pointing default:

The telescope pointing defaults resulting from spatial platform instability or the atmospheric turbulence induce strong effects. In the case of two identical telescopes tilted by $\theta1$ and $\theta2$, a1(θ) and a2(θ) become a(θ-$\theta1$) and a(θ-$\theta2$). $\theta1$ and $\theta2$ being random values, the a(θ-$\theta1$).a(θ-$\theta2$) product can't be known and the data is definitely corrupted.

The figure 8 shows an example of the effect of the telescope pointing default on the observable object (product a(θ-$\theta1$).a(θ-$\theta2$) I(θ)) in the frame-work of our test bench .

For an imaging reconstruction, with this configuration, the image reconstructed would be the observable object equal to the product a(θ).a(θ-$\theta2$).I(θ). In so far as $\theta2$ is unknown, the real image can not be reconstructed.
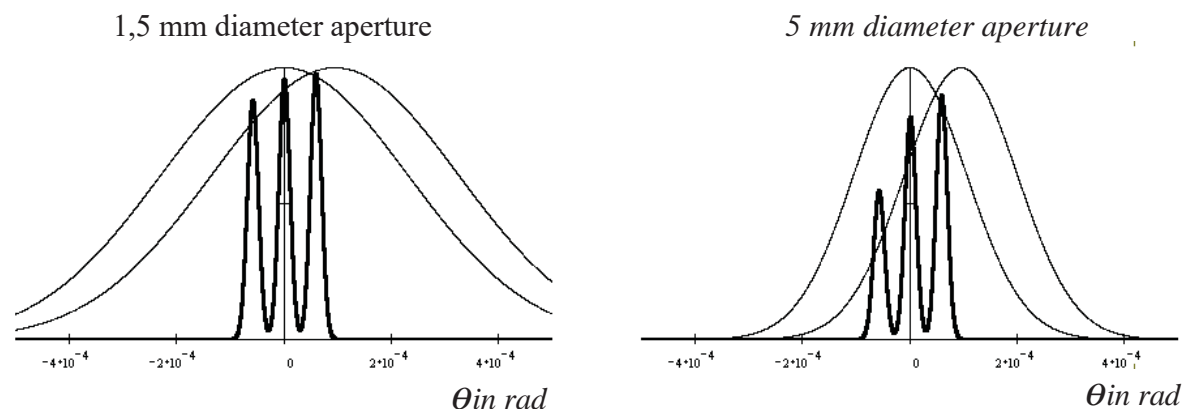
1,5 mm diameter aperture   5 mm diameter aperture

θ in rad   θ in rad

fig 8: effect of pointing default of telescope 2 on the product a(θ).a(θ-θ2).I(θ)
sharp curves: intensity antenna diagram a(θ) and a(θ-θ2)
bold curves: a(θ).a(θ-θ2).I(θ) product

These two graphs show that with a large aperture the corruption of the image is more important than with a small aperture. The original object is always a triplet with the same intensity for each star.

With a 1,5 mm diameter the relative error between the two maximum is 9% and with 5 mm diameter aperture give a 40 % relative error.

4.2-simulation of the corruption on the contrast and phase closure:

The larger is the aperture the narrower is the telescope antenna diagram, the more corrupted is the data with a telescope pointing default. That explanation can be generalised for a 2 dimension array. We simulate for a two dimensional object, the effect of antenna diagram with and without telescope pointing defaults. This following table presents the real value, and simulations of data coming out from the stellar interferometer

Used aperture	Ideal aperture	D = 1.5 mm	D = 5 mm
Contrast 1+ref	0,22	0,24	0,27
Contrast 2+ref	0,11	0,11	0,11
Contrast 1+2	0,54	0,53	0,52
Phase closure	2,56 rad	2,50 rad	2,32 rad

Contrast and phase closure simulation with different aperture diameter, without telescope pointing default.

Used aperture	Ideal aperture	D = 1.5 mm	D = 5 mm
Contrast 1+ref	0,22	0,24	0,27
Contrast 2+ref	0,11	0,07	0,04
Contrast 1+2	0,54	0,55	0,57
Phase closure	2,56 rad	2,64 rad	4,66 rad

Contrast and phase closure simulation with different aperture diameter, with 10 mm focal lens and a 10 arc second telescope pointing default.

These tables show that the phase-closure fluctuation is very important, when a pointing default is occurred. Of course this effect increase when the lens is larger. The ideal aperture is a point like aperture giving a homogenous antenna diagram. The computed contrast and phase closure

confirm that the larger is the telescope the more corrupted is the data. In addition, we can notice that data corruption is very sensitive to a telescope pointing default.

5-CONCLUSION

In a stellar interferometer, modulus and phase-closure data corruption can arise from two matters referring together to pupil antenna diagram. In the frame of aperture synthesis, the object must not be resolved by each telescope as long as the aperture synthesis principle is based on the correlation of electric fields collected by two pupils. The electric field launched into the optical fibre has to characterise the whole object. By using a large antenna diagram, the object image can be fully included into the Airy disk in the focal plane of the telescope. The object is not resolved by each telescope and data is not corrupted.

If each telescope resolve the object , a part of the object information is only contained in the electric field launched in the fibre so that the field correlation (i.e. the fringe contrast) may be biased. This effect can be avoid if all the telescopes point exactly in the same direction. In this configuration, the observed object is only a part of the real object. Experimentally, pointing telescope accurately for all the telescopes is very difficult. A very small pointing error could corrupt the data because each telescope doesn't collect information on the same part of the object, so that the correlation between the two fields decreases.

This theoretical study will be followed by the experimental demonstration of the image corruption induced by antenna diagram effects. In such context, laboratory tests are necessary as long as these effects are steady and possible to quantify. Direct study on the sky would require perfect adaptive optics and tip-tilt systems [Rous 00].

BIBLIOGRAPHIE :

[Dela 00] L.Delage, F Reynaud, A.Lannes : "Laboratory imaging stellar interferometer with fiber
          links", *Aplied optics , vol**39** n°34,(dec 2000)*

[Born 80] M.Born and E.Wolf, *Principles of Optics* 6th edn, 1980.

[Kudi 97] Klaus H Kudielka, "adaptative receive telescope array for laser communications in
          space", Ph D Thesis, Techniche Universitat Wien, 1997.

[Rous 00] G.Rousset, F.Lacombe, P.Puget, E.Gendron, R.Arsenault, P.Kern, D.Rabaud, P.-Y.
          Madec, N.Hubin, G.Zins, E.Stadler, J.Charton, P.Gigan, P.Feautrier, "Status of VLT
          Nasmyth Adaptive Optics System (NAOS) ",*SPIE*, Müchen, march 2000.